Infrared Spectroscopy of Mixed Nitric-Oxide−Carbon-Monoxide Adlayers on Ordered Iridium(111) in Aqueous Solution: A Model Study of Coadsorbate Vibrational Interactions

Catherine Tang,[†,‡] Shouzhong Zou,[†] Mark W. Severson,[§] and Michael J. Weaver

Department of Chemistry, Purdue University, West Lafayette, Indiana 47907; Department of Chemistry, National Tsinghua University, Hsinchu 30043, Taiwan; and Department of Chemistry, Oakland University, Rochester, Michigan 48309

Received: June 12, 1998; In Final Form: August 3, 1998

In-situ infrared reflection−absorption spectra are reported for mixed nitric-oxide−carbon-monoxide adlayers along with the constituent chemisorbates separately as a function of coverage on ordered Ir(111) at 0.4−0.45 V vs standard hydrogen electrode in aqueous 0.1 M $HClO_4$, with the objective of assessing the composition-dependent nature of the coadsorbate vibrational interactions. This substrate−coadsorbate combination provides an informative model system since both chemisorbates appear to bind exclusively in atop (or near-atop) surface sites on the basis of their simple N−O (ν_{NO}) and C−O (ν_{CO}) vibrational fingerprints, and composition-dependent mixed adlayers can readily be formed via partial replacement of saturated irreversible adsorbed NO layers by exposure to dilute CO solutions. Increasing the CO coverage, θ_{CO}, both in the absence and presence of coadsorbed NO, yields marked progressive blueshifts in the ν_{CO} band frequency (ca. 2020−2075 cm^{-1}), attributable chiefly to enhanced dipole−dipole coupling. While adsorption of NO alone exhibited virtually coverage (θ_{NO})-independent ν_{NO} frequencies, ca. 1835 cm^{-1}, indicative of chemisorbate island formation, dilution within mixed CO/NO adlayers yields progressive ν_{NO} redshifts (down to ca. 1790 cm^{-1}). The composition-dependent ν_{CO} and ν_{NO} frequencies within the CO/NO adlayers are consistent with molecular intermixing, as supported by comparison with numerical simulations extracted from conventional dipole-coupling theory, although the observed nonlinear $\nu_{CO}-\theta_{CO}$ dependence suggests the formation of locally enriched CO regions at intermediate compositions. Evidence supporting coadsorbate intermixing is obtained by comparing the composition-dependent CO and NO band absorbances with the dipole-coupling predictions. In particular, the presence of coadsorbed CO yields marked (up to 3-fold) decreases in the NO band absorbance, especially toward lower ν_{NO} values, which arise from band-intensity transfer to neighboring higher-frequency (CO) oscillators. Despite the large (ca. 250 cm^{-1}) difference in ν_{NO} and ν_{CO} singleton frequencies, this striking effect is in approximate agreement with dipole-coupling theory, again presuming molecular CO/NO intermixing. The observed marked increases in the ν_{CO} bandwidth toward lower θ_{CO} values, along with pronounced asymmetric band shapes, are in good agreement with theoretical predictions that include stochastic fluctuations of the local adsorbate population density. Moreover, the larger intermediate-θ_{CO} ν_{CO} bandwidths observed in the presence of coadsorbed NO are also quantitatively accounted for on this basis in terms of coadsorbate intensity transfer. The more broad-based utility of such dipole-coupling analyses for elucidating local interactions within mixed adlayers is considered in light of these findings.

Introduction

Molecular coadsorption is omnipresent in interfacial science, especially in electrochemical systems, so that understanding the nature and consequences of the intermolecular interactions involved is of broad significance.[1] Besides solute−solvent interactions which can modify (or even determine) chemisorbate structure and reactivity at metal−solution interfaces, molecular coadsorption is generally encountered in heterogeneous catalytic systems. Given the sensitivity of adsorbate vibrational properties to their bonding and intermolecular interactions, for model studies it is clearly advantageous to select coadsorbate systems where one or preferably both components provide structure-sensitive spectral fingerprints.[1] A particularly interesting chemisorbate pair from this standpoint is nitric oxide−carbon monoxide. The intramolecular vibrations for both these simple diatomic adsorbates yield intense infrared bands that are highly dependent on the surface bonding and local electrostatic environment. Consequently, the chemisorption of NO and especially CO have been examined in detail by means of infrared reflection−absorption spectroscopy (IRAS) on ordered monocrystalline metals, not only in ultrahigh vacuum (UHV) but recently also in electrochemical environments.[2−4] Comparison of the infrared spectral properties at related metal−UHV and metal−solution interfaces can yield substantial insight into the additional factors that determine the inherently multicomponent nature of the latter systems.[2,3]

We have, therefore, been motivated recently to explore the microscopic nature of mixed NO/CO adlayers on low-index Pt-group metals in aqueous solution by means of IRAS, supplemented by electrochemical (voltammetric) measurements.[5,6] A central objective is to explore the mutual perturbations, especially dipole−dipole coupling, exerted on the chemisorbate vibrational properties by the local coadsorbate environment. One

[†] Purdue University.
[‡] National Tsinghua University.
[§] Oakland University.

10.1021/jp982603r CCC: $15.00
Published on Web 09/30/1998

interesting facet of these electrochemical systems lies in the ability to selectively remove either the CO or NO component of the mixed adlayer by electrooxidation (to CO_2) or electroreduction (to NH_3). The electrode potentials where these processes occur are sufficiently separated in acidic aqueous media (typically by 0.2−0.4 V) to provide a "potential window" where the mixed adlayers are stable. We have focused attention on Pt-group surfaces on which the adsorption of NO is essentially molecular, i.e., where bond dissociation does not occur.[5−7] Studies have been undertaken on Pt(100),[5] Pt(111), Pd(111),[7b] Ir(111), and Ir(110).[7a] Of these faces, Ir(111) is of particular interest for several reasons. A straightforward (non-UHV) annealing procedure is available which yields Ir(111) surfaces displaying a high degree of order, as surmised from both voltammetry and IRAS.[6,8] In particular, both CO and NO display only a single infrared intramolecular stretching band on Ir(111) over a wide range of coverages up to saturation, consistent with chemisorbate binding to only atop (or near-atop) binding sites.[6,7a] The circumstance considerably simplifies the analysis of coverage-dependent vibrational interactions. The vibrational properties of both CO and NO in the coadsorbate layers indicate the occurrence of essentially molecular-level intermixing, rather than the formation of segregated NO and/or CO patches. Last, the fractional coverages of both CO and NO may be obtained by coulometry and the former additionally by infrared spectrophotometry,[9] enabling the adlayer analytical compositions to be determined.

We report herein a detailed investigation into the vibrational spectroscopic and related electrochemical properties of mixed saturated NO/CO adlayers on Ir(111) in aqueous acidic (0.1 M $HClO_4$) solution, especially in relation to the corresponding single-component chemisorbate systems, i.e., coadsorbed with water. The effects of the intermolecular interactions on the infrared spectra are explored by analyzing the vibrational frequency and intensity data as a function of adlayer composition in comparison with the predictions of dynamic dipole-coupling models. The results provide insight into the nature and consequences of such vibrational interactions in this simple intermixed chemisorbate system and also uncover some similarities as well as differences in the coadsorption environment provided by the aqueous solvent and the other chemisorbate.

Experimental Section

Details of the in-situ IRAS instrumentation and procedures are partly outlined in refs 10 and 11. The FTIR spectrometer was a Mattson RS-2 instrument with a custom-built external reflection compartment containing the narrow-band MCT detector. The spectral resolution was 2 cm^{-1}. The glass spectroelectrochemical cell contains a detachable beveled CaF_2 window, forming the base of the vertically oriented cell, which slots into an opening on top of the N_2-purged external optical compartment. This design (kindly provided by Carol Korzeniewski) obviates the need for additional N_2 purging after aligning the cell. The disk electrode, mounted on a glass plunger by wrapping with Teflon tape, was pressed against the CaF_2 window to form the desired spectroelectrochemical thin layer.

The Ir(111) crystal, ca. 1 cm diameter, was procured from the Material Preparation Facility at Cornell University. It was oriented at least within 1°, as verified by X-ray diffraction. It was repolished with diamond paste to 0.25 μm grain size and then flame annealed initially at 1500−1700 °C in an oxy-gas flame for ca. 15 min, to the point where the voltammetric features in 0.1 M $HClO_4$ were unchanged and characteristic of the well-ordered surface.[8,12] The surface was cooled prior to electrochemical or spectroelectrochemical inspection in a fast-flowing H_2/Ar stream, followed by immersion in ultrapure water. Clean transferral to the electrochemical cell was facilitated by retaining a drop of water upon emersion. Successive annealings during each run required heating to 1500−1700 °C for only ca. 10−20 s. [Note that the above surface pretreatment differs from that used in our earlier IRAS study of the Ir(111)/CO system, which entailed forming a protective iodine layer during post-anneal cooling.[13] The present procedure yields a higher-quality ordered surface on the basis of voltammetric and IRAS data (vide infra).[6,8]] Nitric oxide and carbon monoxide (Matheson Gases) were 99.0 and 99.99% min, respectively, the latter packed in an aluminum cylinder (thus avoiding the iron carbonyl contaminants often present in CO stored in steel cylinders). Electrolytes were prepared from concentrated perchloric acid (double distilled, GFS Chemicals) using ultrapure water (Millipore MilliQ). The reference electrode was Ag/AgCl (Bioanalytical Systems), but all electrode potentials quoted here are versus the standard hydrogen electrode (SHE). All measurements were made at room temperature, 23 ± 1 °C.

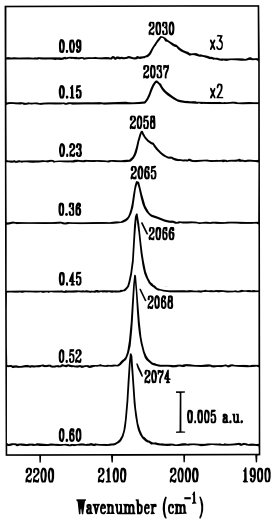

Figure 1. Infrared absorbance spectra (intensities in log absorbance units, au) for various dosed CO coverages, as indicated, on ordered Ir(111) at 0.4 V vs SHE in aqueous 0.1 M $HClO_4$.

Results

IRAS of Separate CO and NO Adlayers. Prior to presenting the IRAS and related electrochemical behavior of the mixed NO/CO adlayers, it is convenient to consider the behavior of CO and NO adsorption separately on Ir(111). We have recently described in detail the coverage-dependent IRAS properties of CO dosed onto Ir(111) in aqueous 0.1 M $HClO_4$,[6] including a comparison with literature data for the corresponding UHV-based system,[14] so that the presentation here is relatively brief. Comparison of the present composition-dependent IRAS data with the predictions of dipole-coupling models is undertaken in the Discussion section.

Figure 1 shows infrared absorbance spectra obtained in the C−O stretching (ν_{CO}) region for a sequence of increasing dosed CO coverages, θ_{CO}, onto Ir(111) at 0.4 V vs SHE in 0.1 M $HClO_4$. The irreversibly adsorbed CO adlayers were formed by briefly (1−3 s) bubbling in CO followed by argon sparging, removing almost all the solution CO before forming the spectroelectrochemical thin layer. The ν_{CO} spectra for a given dosed adlayer were obtained by typically acquiring 100 interferometer scans at the desired electrode potential (consuming

ca. 20 s) followed by a "reference spectrum" measured immediately thereafter at 0.75 V, where the adsorbed CO is oxidized entirely to CO_2. This now-standard potential-difference infrared (PDIR) procedure[10,11] removes the bulk solvent and other unwanted infrared features, yielding the desired ν_{CO} surface component along with a sharp opposite-polarity band at 2345 cm^{-1} due to the CO_2 product trapped in the spectroelectrochemical thin layer. As documented recently elsewhere,[6,9] the CO_2 band intensities together with a coulometric analysis yield reliable (and accurate) values of the CO packing density, Γ (mol cm^{-2}), and hence the fractional CO coverage, θ_{CO}, given the metal atomic density on Ir(111), 1.57×10^{15} atoms cm^{-2}. The saturated coverage, θ_{CO}^{sat}, is 0.60 ($\pm$0.05). The electrode potential chosen for Figure 1, 0.4 V, is slightly lower than that, 0.45 V, utilized for the mixed CO/NO adlayers described below. The latter potential is an optimal choice to avoid CO electrooxidation as well as NO electroreduction. However, *pure* CO adlayers dosed to intermediate coverages can undergo slow electrooxidation at 0.45 V, which can alter the precise form of the θ_{CO}-dependent ν_{CO} spectra, depending on the IRAS measurement time scale. Since the intrinsic differences between the ν_{CO} spectra at 0.4 and 0.45 V are almost negligible (the former ν_{CO} frequencies are only 1.5−3 cm^{-1} lower), we utilize instead the slightly lower dosing potential of 0.4 V in Figure 1.

A single ν_{CO} band is evident in Figure 1, which blueshifts markedly, from ca. 2020−2075 cm^{-1}, with increasing θ_{CO} up to saturation (0.05−0.6). This behavior is indicative of increasing dipole−dipole coupling toward higher θ_{CO}, acting to progressively blueshift the observed ν_{CO}^{p} values.[6,14,15] As outlined in ref 6, the θ_{CO}-dependent peak frequencies, ν_{CO}^{p}, are closely similar to $\nu_{CO}^{p}-\theta_{CO}$ data obtained for CO on Ir(111) in UHV, also at ambient temperature,[14] after corrections are made for differences in the surface potentials in the two environments (cf., ref 3). We consider below the relationship of the coverage-dependent ν_{CO} frequency, intensity, and band shape data, referring to CO coadsorbed with water, to the corresponding behavior observed for saturated CO/NO mixtures. The ν_{CO} frequency-electrode potential dependence is complicated somewhat by hysteresis observed upon sweeping to low potentials, 0 V, within the "hydrogen adsorption" region, and return.[6] However, taking the portion of the $\nu_{CO}^{p} - E$ data obtained at potentials, 0.2−0.45 V, where the adlayer is stable and only water coadsorption occurs yields $d\nu_{CO}^{p}/dE$ values of about 60 cm^{-1} V^{-1} at low coverages, $\theta_{CO} \approx 0.1$, decreasing with increasing coverage to 35 cm^{-1} V^{-1} for the saturated adlayer.

Turning now to NO adsorption, Figure 2 shows infrared absorbance spectra in the N−O stretching (ν_{NO}) region obtained for a sequence of increasing dosed NO coverages, θ_{NO}, on Ir(111) at 0.45 V in 0.1 M $HClO_4$. The "reference spectrum", required as before to remove the bulk-phase interferences, was obtained after stepping the potential to 0.05 V to reductively remove the NO adlayer. The irreversibly adsorbed NO adlayers were formed by immersing the freshly annealed Ir(111) surface in deaerated 0.1 M $HClO_4$ containing NO for ca. 5−30 s (using diluted NO solutions to achieve lower coverages). The crystal was then transferred (protected by a drop of solution, as usual) into the spectroelectrochemical cell containing 0.1 M $HClO_4$ at 0.45 V. The θ_{NO} value, varied by altering the exposure time to the NO-containing solution, was determined from the coulometric charge contained under the broad voltammetric peak observed at about 0.2−0.3 V (vide infra). Assuming a five-electron reduction process (i.e., that ammonia is formed, cf., ref 4) yields a saturated NO coverage, $\theta_{NO}^{sat} \approx 0.45$ ($\pm$0.1).

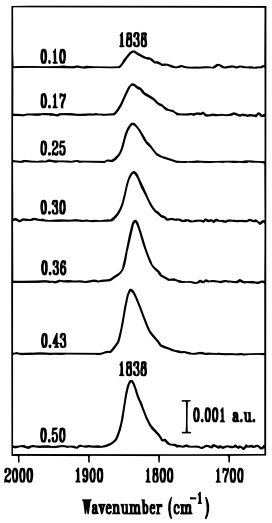

Figure 2. Infrared absorbance spectra for various dosed NO coverages, as indicated, on Ir(111) at 0.45 V in aqueous 0.1 M $HClO_4$.

However, this coulometric estimate is only approximate since double-layer charging corrections can be problematic[9] and, moreover, it is not clear that the adsorbed NO undergoes a "total" five-electron reduction. (For example, the partial formation of N_2, a $2e^-$ product, would on this basis yield a marked increase in the θ_{NO}^{sat} estimate for a given cathodic charge.) Consequently, we select here a θ_{NO}^{sat} value, 0.5, which is consistent with the relative saturation coverages determined for NO versus CO on other surfaces [e.g., Pt(100)[16]], including coulometric estimates for several Pt-group electrodes.[4] The θ_{NO} values given for the subsaturated NO adlayers in Figure 2 were, therefore, obtained from the coulometric reduction charges relative to the saturated value assuming $\theta_{NO}^{sat} = 0.5$. Fortunately, this (uncertain) choice is not important for the present purposes since only relative values are needed here.

Unlike the θ_{CO}-dependent ν_{CO} data, the corresponding NO spectra yield a single ν_{NO} band centered at about 1835 cm^{-1} at 0.45 V, the peak frequency (ν_{NO}^{p}) being almost *independent* of θ_{NO} over the entire coverage range accessed (ca. 0.1−0.5, Figure 2). The peak frequency increased toward higher potentials with a slope, $d\nu_{NO}^{p}/dE = 60$ cm^{-1} V^{-1}, that is also almost independent of θ_{NO}. This behavior provides strong evidence that the NO adlayer forms close-packed nanoscale (or larger) islands over this θ_{NO} range, so that the "local" (microscopic) coverage, θ_{NO}^{loc}, remains high even when the "average" (measured) θ_{NO} becomes much lower. The formation of such islands will, therefore, yield strong dipole−dipole coupling and, hence, blueshifted ν_{NO} frequencies which are largely independent of θ_{NO}. A similar situation has been encountered for CO dosing on Pt(111) with coadsorbed water[10] and commonly during the electrooxidation of CO adlayers on Pt-group electrodes, since the process occurs preferentially at the edges of CO nanoscale "islands".[17,18] Another anticipated consequence of such chemisorbate island formation is that the integrated ν_{CO} (or ν_{NO}) band absorbance, A_i, should be proportional to θ_{CO} (or θ_{NO}), as is often observed.[10] The A_i values for the ν_{NO} spectra such as in Figure 2, A_{NO}, are indeed proportional to θ_{NO}, the latter as estimated from reduction coulometry.

Voltammetry of CO/NO Adlayers. It is instructive to examine the voltammetric oxidation and reduction of the CO/NO adlayer components adsorbed separately in relation to the corresponding behavior in the coadsorbate matrix. Such information provides a necessary guide to the electrode potential

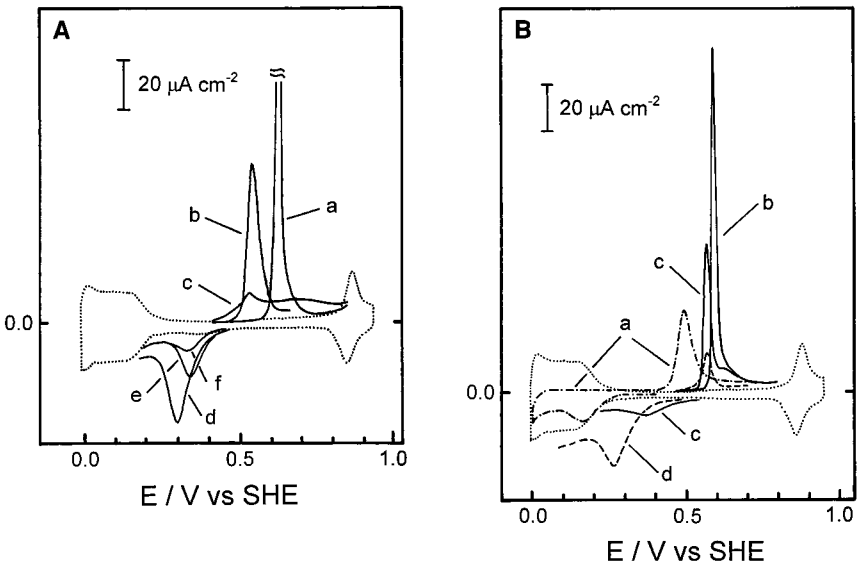

Figure 3. (A) Voltammograms (10 mV s^{-1}) for the oxidation of selected dosed coverages of CO (a−c) and for the reduction of NO (d−f) on Ir(111) in 0.1 M $HClO_4$ (see text). The dotted trace is a cyclic voltammogram for clean Ir(111), i.e., in the absence of either chemisorbate. (B) Selected voltamograms (10 mV s^{-1}) for saturated mixed CO/NO adlayers on Ir(111) in 0.1 M $HClO_4$. Trace a is a cathodic−anodic voltammogram, i.e., for NO reduction followed by CO oxidation ($\theta_{CO} \approx 0.35$). Traces b−d refer to CO oxidation followed by NO reduction, for initial θ_{CO} values of ca. 0.4, 0.3, and 0.05, respectively (see text). (Note that the NO reduction segment for b is not shown for clarity; it is similar to c.

region within which the mixed adlayers as well as the individual components are stable to oxidation and/or reduction.

Part A of Figure 3 contains anodic and cathodic voltammograms at 10 mV s^{-1} for various dosed coverages of carbon monoxide (a−c) and nitric oxide (d−f) on Ir(111) in 0.1 M $HClO_4$. The dotted trace was obtained in the absence of either chemisorbate; the reversible features at 0 to −0.2 and 0.8 V are characteristic of adsorbed hydrogen and oxygen formation/removal on ordered Ir(111) in 0.1 M $HClO_4$.[8,12] Curve a was obtained for a saturated CO adlayer ($\theta_{CO} \approx 0.6$), dosed at 0.4 V. The very sharp onset of oxidation current at 0.57 V and narrow voltammetric peakwidth (20 mV) are characteristic of a "nucleation-growth" type of mechanism involving the reaction between the CO and oxidant (adsorbed OH or water) spreading outward from nucleation centers (such as adlayer defect sites) where the latter reactant can bind.[19] Traces b and c in Figure 3A are the corresponding anodic voltammograms obtained for intermediate and lower CO dosages ($\theta_{CO} \approx 0.4$ and 0.15, respectively). Compared with a, the voltammetric waves in b and especially c are broader, with the onset of reaction shifting by ca. 0.15 V to lower potentials (vide supra). This behavior is commonly seen for voltammetric CO oxidation on ordered Pt-group electrodes[20] and is attributable to the markedly greater access of the coadsorbed oxidant to the CO when the latter forms an "open" subsaturated molecular array on the surface. We will present elsewhere a combined IRAS−dipole coupling analysis of CO adlayer oxidation on Ir(111), with the objective of elucidating the nanoscale CO structures formed during this process.[21]

The cathodic voltammogram d was obtained for a saturated NO adlayer at 0.45 V. Electroreduction yields a broader voltammogram with a shallow onset than that for saturated CO electrooxidation. As mentioned above, the reaction mechanism and even the precise product distribution for adsorbed NO reduction (NH_4^+, N_2 formation) are incompletely known, although the process clearly involves protons and possibly adsorbed H atoms.[4] Traces e and f in Figure 2A refer to a pair of lower-dosed NO coverages. Relative to CO oxidation, the onset of adsorbed NO reduction is only mildly affected by the initial NO coverage. Interestingly, NO electroreduction on Ir(111) occurs at higher potentials than on most Pt-group surfaces in acidic media.[4]

Part B of Figure 3 shows representative voltammograms, again at 10 mV s^{-1}, for mixed CO/NO adlayers on Ir(111). A basic issue addressed by these results concerns the effect of coadsorbed CO on the voltammetric removal of NO and vice versa. Trace a refers to the initial reduction of NO (initial negative-going potential sweep) in a CO/NO mixture ($\theta_{CO} \approx$ 0.35), followed by CO oxidation. The presence of the CO matrix is observed to inhibit NO reduction, shifting the cathodic wave to significantly (0.1−0.2 V) lower potentials. Indeed, in some cases it is difficult to disentangle the cathodic current for the latter stages of NO reduction from that for hydrogen adsorption and even H_2 evolution, hampering coulometric measurements. Traces b-d in Figure 3B show voltammograms for the oxidation of adsorbed CO (initial positive-going potential sweep) followed by NO reduction in saturated CO/NO adlayers increasingly dilute in CO (θ_{CO} values of about 0.4, 0.3, and 0.05, respectively). Interestingly, the CO oxidation peaks are sharper in the presence of the NO matrix rather than coadsorbed water, with higher (up to 0.1 V) onset potentials than those observed at comparable θ_{CO} values for dosed CO adlayers in the absence of NO. This behavior indicates that the coadsorbed NO provides a less-favorable environment for adsorbed CO electrooxidation than does coadsorbed water. This point is significant since it is conceivable that NO, in addition to water, could provide a viable oxidant for adsorbed CO.

IRAS of Mixed CO/NO Adlayers. Of central interest here is exploring the nature of composition-dependent ν_{CO} and ν_{NO} spectra within the mixed CO/NO adlayers on Ir(111) in relation to the corresponding coverage-dependent behavior of the separate chemisorbates. A typical set of IRAS data obtained for a sequence of mixed CO/NO adlayer compositions at 0.45 V is shown in Figure 4. Similarly to the voltammetric data, the mixed CO/NO adlayers were seen by IRAS to be stable over the potential region 0.35−0.5 V or so, the limits depending somewhat on the adlayer composition. The spectra were obtained similarly to those in Figures 1 and 2 but by recording the "reference spectrum" after stepping the potential sequentially to 0.75 and 0.05 V to remove the adsorbed CO and NO

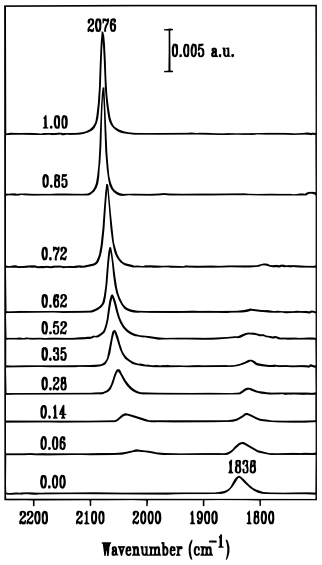

Figure 4. Infrared absorbance spectra for saturated mixed CO/NO adlayers on Ir(111) at 0.45 V vs SHE in 0.1 M $HClO_4$ as a function of adlayer composition, given as "fractional CO coverages" X_{CO} (see text).

components, respectively. The values indicated beside each spectrum in Figure 4 are the "fractional CO coverages" in the mixture, X_{CO}, defined by $X_{CO} = \theta_{CO}/\theta_{CO}^{sat}$. Interestingly, the X_{CO} values were found to be related simply to the corresponding "fractional NO coverages", X_{NO} ($= \theta_{NO}/\theta_{NO}^{sat}$), by $X_{CO} = (1 - X_{NO})$. This approximate relationship was deduced from a slope of -1 consistently extracted from plots of X_{CO} versus X_{NO}, these quantities being obtained by spectrophotometry and coulometry, respectively (vide supra). Besides indicating that the mixed NO/CO adlayers form an essentially "ideal" solid solution, those findings provide further indication of their stability toward chemical (or electrochemical) decomposition, at least at electrode potentials close to 0.45 V, where the voltammetry (Figure 3B) indicates the lack of either CO electrooxidation or NO reduction.

Careful inspection of the infrared spectra in Figure 4 reveals at least two key features. First, both the higher and lower frequency bands are redshifted markedly toward smaller X_{CO} and X_{NO} values, respectively, i.e., upon dilution of one chemisorbate by the other component. These frequency−composition variations for the CO and NO components at 0.45 V are plotted as ν_{CO}^{p} versus X_{CO} and ν_{NO}^{p} versus X_{NO} in Figures 5 and 6 (filled circles). Included for comparison in Figures 5 and 6 (open circles) are the corresponding $\nu_{CO}^{p}-X_{CO}$ and $\nu_{NO}^{p}-X_{NO}$ plots obtained for CO and NO, respectively, dosed *separately* on "clean" Ir(111) in 0.1 M $HClO_4$ at 0.4 and 0.45 V, respectively (vide supra), extracted from spectra such as in Figures 1 and 2. Comparison between the $\nu_{CO}^{p}-X_{CO}$ plots in the presence of coadsorbed water and NO (open and filled circles, respectively, Figure 5) shows that both environments engender similar ν_{CO} frequency redshifts toward lower X_{CO} values. For NO, however, the marked ν_{NO}^{p} redshifts observed toward lower X_{NO} in the coadsorbed CO matrix contrast the X_{NO}-independent ν_{NO}^{p} values obtained in the presence of coadsorbed water (Figure 6, vide supra). As discussed below, these composition-dependent ν_{CO} and ν_{NO} band frequencies are indicative of the progressive attenuation of the dipole coupling-induced blueshifts by increasingly diluting the oscillator by the other chemisorbed species. Examination of the $\nu_{CO}^{p}-E$ and $\nu_{NO}^{p}-E$ dependencies within the mixed adlayers was hampered by the narrow potential range of their stability.

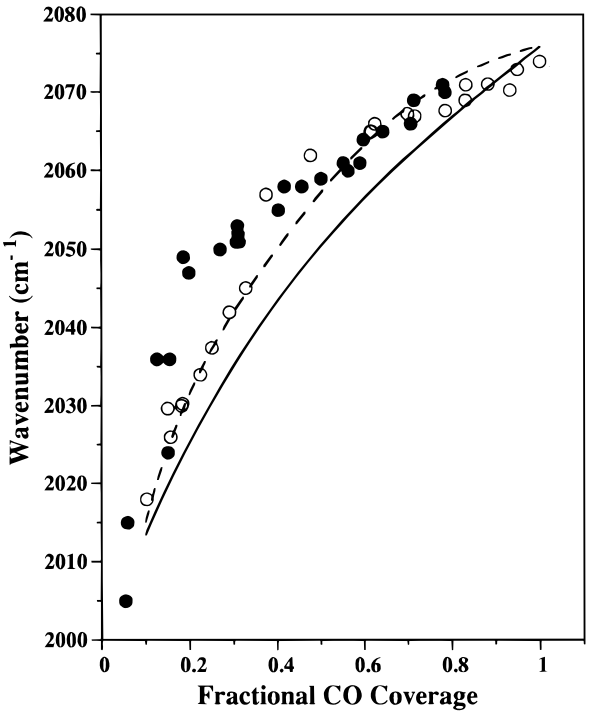

Figure 5. Plots of the peak ν_{CO} frequency, ν_{CO}^{p}, versus the fractional coverage, X_{CO}, for CO adsorbed on Ir(111) in 0.1 M $HClO_4$ in the absence (○) and presence (●) of coadsorbed NO (at 0.4 and 0.45 V, respectively). The dashed and solid traces are the corresponding predicted $\nu_{CO}^{p}-X_{CO}$ plots extracted from dipole-coupling simulations (see text for input parameters, etc).

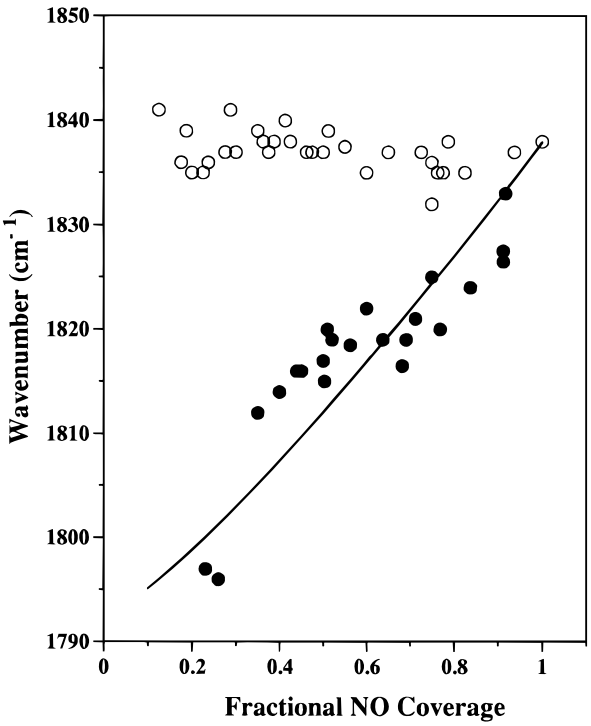

Figure 6. Plots of the peak ν_{NO} frequency, ν_{NO}^{p}, versus the fractional coverage, X_{NO}, for NO adsorbed on Ir(111) in 0.1 M $HClO_4$ at 0.45 V in the absence (○) and presence (●) of coadsorbed CO. The solid trace is the corresponding predicted $\nu_{NO}^{p}-X_{NO}$ plot for the latter case extracted from dipole-coupling simulations (see text for input parameters).

The second key feature evident in the spectra in Figure 4 concerns the composition-dependent band intensities. Dilution of the higher-frequency (CO) component (i.e., toward lower X_{CO}

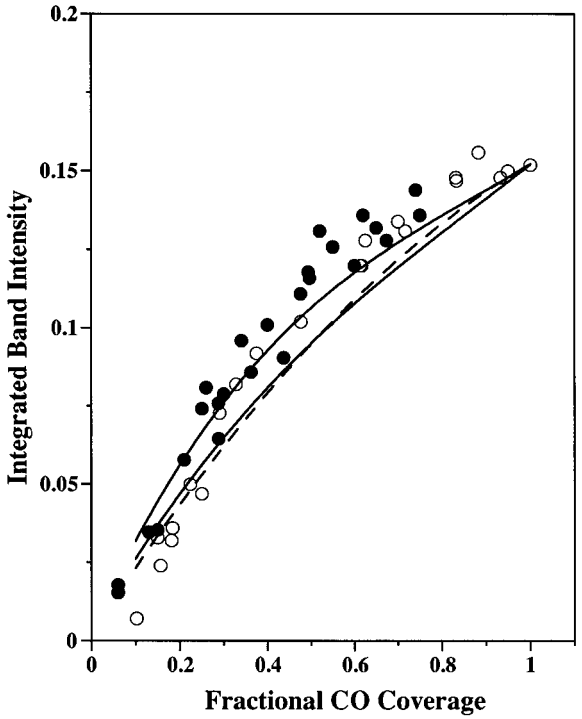

Figure 7. As in Figure 5 but for integrated CO band absorbance, A_{CO}. The dashed trace and the solid traces are the corresponding predicted $A_{CO}-X_{CO}$ plots in the absence and presence of coadsorbed NO, respectively, obtained from dipole-coupling simulations (see text for input parameters).

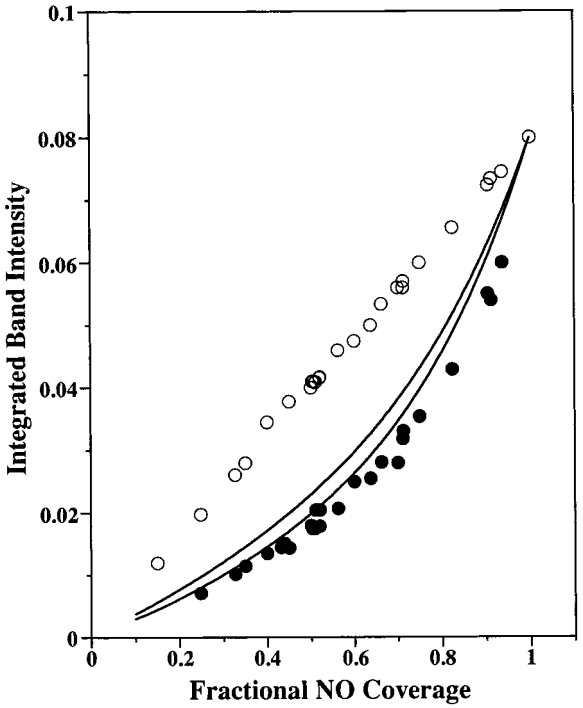

Figure 8. As in Figure 6 but for integrated NO band absorbance, A_{NO}. The solid traces are a pair of predicted $A_{NO}-X_{NO}$ plots extracted from dipole-coupling simulations (see text for input parameters).

values) yields only gradual progressive diminutions in the integrated band absorbance, A_{CO}. However, the lower-frequency (NO) component undergoes a much steeper attenuation in the integrated band absorbance, A_{NO}, toward lower X_{NO} [i.e., $(1 - X_{CO})$] values. These differences are clearly evident in the plots of the integrated band absorbance versus fractional coverage in the CO/NO mixture for the CO and NO components shown (filled circles) in Figures 7 and 8, respectively. (The A_i values are given in au cm^{-1}, where au are log absorbance units.) The open circles in Figures 7 and 8 are the corresponding X-dependent A_i values obtained for the ν_{CO} and ν_{NO} bands, respectively, in the presence of coadsorbed water rather than the other chemisorbate (cf., format for Figures 5 and 6). The $A_{CO}-X_{CO}$ plot obtained in the presence of coadsorbed NO is not greatly different from that with coadsorbed water (Figure 7), although the former exhibits a slightly greater curvature resulting from enhanced A_{CO} values at intermediate CO coverages. In contrast, however, the $A_{NO}-X_{NO}$ plot for the NO/CO mixtures exhibits markedly (2−3-fold) *depressed* A_{NO} values toward intermediate and low NO coverages in comparison with that in the absence of CO (Figure 8). As detailed further below, these marked behavioral differences in the composition-dependent ν_{CO} and ν_{NO} band intensities in the CO/NO mixtures signal the presence of substantial "intensity-transfer" effects from the lower- to higher-frequency oscillator components arising from dipole−dipole coupling.[7a]

As mentioned at the outset, an invaluable feature of the present CO/NO adlayers is the opportunity to selectively remove one of the chemisorbates by electrochemical oxidation or reduction. In particular, the ready oxidative removal of the CO component enables the degree of ν_{NO} band suppression induced by this coadsorbate to be directly monitored. Figure 9(A−D) show four pairs of ν_{CO}/ν_{NO} spectra obtained at 0.45 V before and after CO removal (lower and upper partners, respectively) for decreasing X_{CO} values (0.7, 0.45, 0.25, and 0.08, respectively). The increasing suppression of ν_{NO} band intensity in the NO/CO mixture, as evaluated by the ratio of band absorbances in the presence and absence of CO, $A_{NO}/A_{NO}°$, toward higher X_{CO} (i.e., lower X_{NO}) is clearly evident in Figure 9. Indeed, the $A_{NO}/A_{NO}°$ values approach 0.3 or so for low X_{NO} values. The significance of these findings for understanding vibrational interactions within such intermixed adlayers is considered further below.

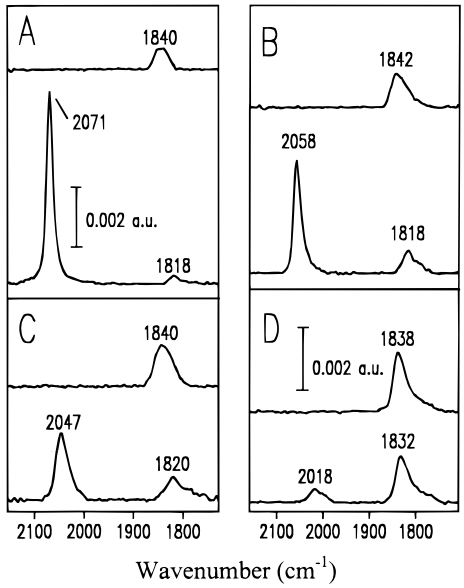

Figure 9. Effect of electrooxidatively removing CO component on infrared spectra of saturated mixed CO/NO adlayers on Ir(111) at 0.45 V in 0.1 M $HClO_4$. Key to fractional CO coverages, X_{CO}: A, 0.7; B, 0.45; C, 0.25; D, 0.08.

In addition to the band frequencies and absorbances, another spectral parameter which is sensitive to the local adsorbate environment is the bandwidth, expressed usually as the full width at half maximum, $\Delta\nu_{1/2}$. Given that the ν_{CO} band shape

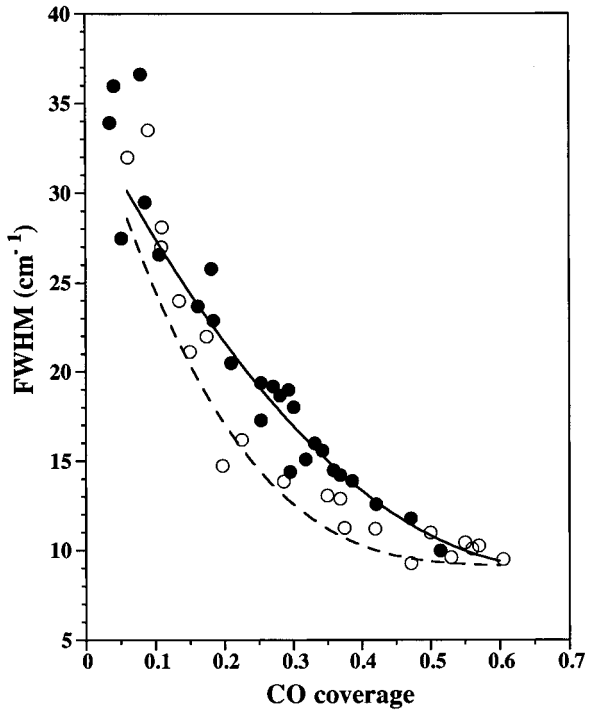

Figure 10. Bandwidth of ν_{CO} band, given as full width at half-maximum, $\Delta\nu_{1/2}$, plotted versus CO coverage, θ_{CO}, on Ir(111) in 0.1 M $HClO_4$ in the absence (○) and presence (●) of coadsorbed NO (at 0.4 and 0.45 V, respectively). The dashed and solid traces are the corresponding predicted $\Delta\nu_{1/2}-\theta_{CO}$ plots extracted from dipole-coupling simulations (see text for input parameters).

can be readily characterized over a wide composition range in both the presence and absence of coadsorbed NO, the comparative examination of θ_{CO}-dependent $\Delta\nu_{1/2}$ values under these conditions might be expected to shed further light on coadsorbate interactions. Figure 10 shows such $\Delta\nu_{1/2}-\theta_{CO}$ plots for CO adsorbed with water (spectra as in Figure 1) and with coadsorbed NO (as in Figure 3), shown as open and filled circles, respectively. The $\Delta\nu_{1/2}$ values are seen to decrease in a comparable fashion in these two environments with increasing θ_{CO} , from 35 to 40 cm^{-1} at low CO coverages to 9−10 cm^{-1} close to saturation. This behavioral similarity in the adsorbed water and NO matrixes is at first sight surprising, since the large $\Delta\nu_{1/2}$ values observed when the CO molecules are surrounded with coadsorbed water (at low θ_{CO}) might be attributed to solvation-induced inhomogeneous band broadening. However, a further behavioral similarity is evident upon inspection of the low-θ_{CO}:ν_{CO} spectra in Figures 1 and 3 in that both the coadsorbed water and NO environments yield band shapes displaying a marked "tail" toward lower wavenumbers. This behavior is discussed in relation to dipole-coupling predictions in the next section.

Discussion: Comparison with Theoretical Dipole-Coupling Predictions

As a starting point in understanding the CO/NO adlayer interactions, it is useful to discuss the coverage-dependent nature of the individual chemisorbate adlayers as deduced from IRAS data. The large θ_{CO}-induced blueshifts in the ν_{CO} band frequency (Figure 1), plotted in Figure 5 (open circles), are similar to those observed for CO dosed onto Ir(111) in UHV.[14] As shown by means of $C^{18}O/C^{16}O$ isotope measurements for the latter system,[14] this $\nu_{CO}{}^{p}-\theta_{CO}$ dependence is due primarily to the increasing effects of dynamic dipole−dipole coupling. (The corresponding measurements for the electrochemical system were precluded by the high cost of $C^{18}O$; the cheaper isotope ^{13}CO yielded an insufficient mass-induced change in the ν_{CO} frequency.[6,13]) Significantly, however, the absorbance-coverage ($A_{CO}-X_{CO}$) plot for CO coadsorbed with water (open circles, Figure 7) exhibits a distinctly different shape to that for the corresponding solvent-free UHV-based system.[14] The latter has a ca. 2-fold larger $A_{CO}-X_{CO}$ slope at low coverages, leading to a plateau for $X_{CO} > 0.5$. While the $A_{CO}-X_{CO}$ dependence for the electrochemical system is, therefore, decidedly less nonlinear, the plot nevertheless exhibits pronounced curvature, with slopes that decrease by 2-fold toward higher X_{CO} (Figure 7).

We have interpreted these differences in terms of X_{CO}-dependent dielectric screening of the CO oscillators by the surrounding solvent.[6] This effect arises from the diminution in the effective dynamic dipole moment, or "vibrational polarizability", of the ν_{CO} vibration caused by its interaction with the polarizable "electron cloud" within the surrounding molecules.[15,22,23] At low θ_{CO}, then, the CO adsorbate will experience dielectric screening chiefly from nearest-neighbor solvent molecules, changing progressively toward high θ_{CO} to screening instead by the surrounding chemisorbate. Since CO has a larger electronic polarizability than water (vide infra), the degree of dielectric screening increases toward high θ_{CO}, accounting for the observed $A_{CO}-\theta_{CO}$ curvature. (The more nonlinear $A_{CO}-\theta_{CO}$ behavior observed for the UHV system is consistent with the anticipated near-absence of screening at low coverages.[6]) Similarly to ref 6, we utilize here a theoretical analysis involving numerical simulations based on dipole−dipole coupling models in order to elucidate the nature of the vibrational interactions within both the pure and mixed chemisorbate adlayers on a unified basis.

Most procedural details of the dipole-coupling calculations undertaken here are described in ref 24. Briefly, the chemisorbate layer was modeled as a large (100−300 molecule) hexagonal array with $\theta = 0.6$, the (equivalent) sites being filled randomly with CO and/or NO molecules to yield the desired fractional coverages. (While other packing arrangements were considered, these yielded similar simulated spectra). The band frequencies and relative intensities were then calculated as described in ref 24, essentially following the method of Greenler and co-workers[25] with the use of periodic boundary conditions. The chemisorbate dipoles were presumed to lie 0.8 D above the image plane,[24] and the required vibrational and electronic polarizabilities, α_v and α_e, respectively, were selected partly by fitting the simulated $\nu_{CO}{}^{p}-X_{CO}$ and $\nu_{NO}{}^{p}-X_{NO}$ results to the experimental data. [The $\nu_{NO}{}^{p}-X_{NO}$ data for the pure NO adlayer were not included in the fitting procedure since the coverage-invariant $\nu_{NO}{}^{p}$ values (Figure 6, open circles) are indicative of extensive adsorbate clustering rather than random site-filling (vide supra).] It should be noted that this procedure implicitly assumes that the dynamic dipole-coupling, rather than "static" (or "chemical"), contributions determine the coverage-dependent band frequency shifts. (While this is probably not entirely true, the former component forms the predominant contribution to the θ_{CO}-dependent ν_{CO} frequency at the Ir(111)−UHV interface.[14]) Each simulated spectrum was generated as a Lorentzian band, typically with $\Delta\nu_{1/2} = 5$ cm^{-1}, the process being repeated a number of times (ca. 100) to yield the final average spectra (cf., ref 26).

The dashed curves shown in Figures 5 and 7 are typical simulated $\nu_{CO}{}^{p}-X_{CO}$ and $A_{CO}-X_{CO}$ plots obtained for the variable-coverage pure CO adlayers in this fashion. Specifically,

the vibrational parameters used in this simulation were $\alpha_e(CO) = 2.5$ Å^3, $\alpha_e(NO) = 2.0$ Å^3, $\alpha_v(CO) = 0.41$ Å^3, $\alpha_v(NO) = 0.2$ Å^3, $\alpha_e(H_2O) = 1.5$ Å^3, $\nu_{CO}{}^s = 2000$ cm^{-1}, $\nu_{NO}{}^s = 1800$ cm^{-1}. The last two quantities are the ν_{CO} and ν_{NO} "singleton frequencies", i.e., the low-coverage limiting values, where dipole coupling is essentially absent. [While the former was obtained from the low-θ_{CO} data (open circles, Figure 5), the latter was estimated partly from the data for the Ir(110)/NO system.[27]] The $\alpha_e(CO)$ value was selected as being characteristic of adsorbed CO,[22,29] and the α_e value for water is that determined from dielectric and optical refraction measurements.[30] The $\alpha_v(CO)$ value was chosen to provide a reasonable match of the simulated $\nu_{CO}{}^p-X_{CO}$ curves to the experimental data. The $\alpha_v(NO)$ value, 0.2 Å^3, was selected partly so to yield reasonable fits to the $A_{NO}-X_{NO}$ as well as $\nu_{NO}{}^p-X_{NO}$ data (see below). It was also assumed that $\alpha_v(water) = 0$, i.e., the water vibrational modes do not contribute significantly to the dynamic dipole coupling involving the ν_{CO} or ν_{NO} oscillators.

While the fit is far from ideal, the calculated plot (dashed curve) provides a reasonable facsimile of the experimental $\nu_{CO}{}^p-X_{CO}$ behavior for CO in the presence of coadsorbed water (open circles, Figure 5). The substantial $\nu_{CO}{}^p$ blue shifts seen toward higher CO coverages reflect the progressively stronger dipole−dipole coupling between neighboring chemisorbate molecules as their average separation distance decreases. The corresponding match to the $\nu_{CO}{}^p-X_{CO}$ data in the presence of coadsorbed NO (solid curve and filled circles, Figure 5) is somewhat inferior in that the experimental points form a decidedly more "bowed" curve. The somewhat (5−10 cm^{-1}) higher $\nu_{CO}{}^p$ values observed toward lower-intermediate X_{CO} values for CO coadsorbed with NO rather than water (Figure 5) may well reflect the presence of small CO aggregates or other molecularly nonrandom CO/NO mixing (see discussion below). However, the overall similarity in the $\nu_{CO}{}^p-X_{CO}$ plots in these two environments, especially the steep slopes observed at low X_{CO}, strongly suggests that the CO/NO adlayers are largely intermixed.

Similar comments also apply to the $A_{CO}-X_{CO}$ data in Figure 7. The match between the experimental points for CO/water coadsorption (open circles) and the theoretical predictions (dashed line) is again reasonable. Two calculated plots (solid curves) are shown for comparison with the experimental data for the CO/NO mixtures (solid circles). The lower trace refers to $\alpha_e(NO) = 2.0$ (as above), and the upper, more bowed, trace was obtained with $\alpha_e(NO) = 1.5$. The use of the smaller NO polarizability is seen to improve the fit with experiment and also accounts for the slightly higher A_{NO} values, which are observed at intermediate X_{CO} values in the CO/NO versus the CO/water coadsorption environments. Altering the NO electronic polarizability in this manner, however, had no significant effect on the calculated $\nu_{CO}{}^p-X_{CO}$ curves (hence, the inclusion of only one solid trace in Figure 5).

Dipole-coupling simulations were also undertaken for nonrandom CO/NO mixtures in order to mimic the possible occurrence of some degree of clustering on the composition-dependent spectral behavior. In essence, the procedure involved a degree of preferential filling of a site with nearest-neighbor CO's with another CO rather than NO. This tactic yields some degree of nonrandom variations of "local" CO (and NO) concentrations and, hence, a variable extent of "mild adlayer segregation." As expected, the procedure yielded $\nu_{CO}{}^p-X_{CO}$ plots that display greater curvature than that calculated for random CO/NO mixtures (solid trace) in Figure 5, thereby coming closer to matching the experimental data (filled circles). A reasonable match was obtained at $X_{CO} = 0.5$, for example, when the average number of CO nearest-neighbors surrounding a given CO molecule was about 3.6 rather than the "random" value of 3.0 (for hexagonal packing). The increased $\nu_{CO}{}^p-X_{CO}$ curvature resulting from such nonrandom arrays can be understood simply from the greater degree of CO dipole−dipole coupling characterizing the locally CO-enriched regions. The shape of the corresponding calculated $A_{CO}-X_{CO}$ plots is less sensitive to the inclusion of such mild "clustering", although slightly greater curvature is predicted, approximately in harmony with the experimental data (Figure 7). However, while the experimental occurrence of mildly nonrandom CO/NO mixing can be reasonably surmised on this basis, the additional adjustable parameters required in the calculational procedure make such experiment−theory curve fitting only suggestive rather than conclusive. [Interestingly, nonetheless, fitting the markedly more nonlinear $A_{CO}-X_{CO}$ behavior observed for CO dosed alone on Ir(111) in UHV (vide supra)[14] with dipole-coupling predictions requires the inclusion of some adsorbate "clustering" at intermediate coverages.]

Examination of the experimental $\nu_{NO}{}^p-X_{NO}$ (Figure 6) and especially the $A_{NO}-X_{NO}$ behavior (Figure 8) for the CO/NO adlayer in relation to the theoretical predictions is also informative. The calculated $\nu_{NO}{}^p-X_{NO}$ curve for the CO/NO mixtures (solid trace) mimics the substantial X_{NO} dependence of the $\nu_{NO}{}^p$ values (filled circles, Figure 6) reasonably well. This finding provides further support to the notion that the CO/NO adlayers are largely molecularly intermixed. We refrain from including a calculated $\nu_{NO}{}^p-X_{NO}$ curve for NO coadsorbed with water. This is because, as already noted, the near θ_{NO}- invariant $\nu_{NO}{}^p$ values (open circles, Figure 6) indicate that NO/water adsorption on Ir(111) involves the formation of locally high NO coverages rather than random-site occupation, so that the dipole coupling-induced $\nu_{NO}{}^p$ blueshift is essentially maintained down to low average ν_{NO} (and X_{NO}) values. Apparently, then, the addition of adsorbed CO to the variable−X_{NO} NO adlayers largely dissipates these (likely large) NO clusters, even though as just noted some nonrandom CO/NO intermixing is likely to occur.

Of particular significance is the $A_{NO}-X_{NO}$ dependence observed in the CO/NO mixtures (Figure 8). Interestingly, the markedly downward-bowed shape of the experimental $A_{NO}-X_{NO}$ plot (filled circles) is reasonably well matched by the calculated traces (solid lines). As in Figure 7, the two traces shown refer to $\alpha_e(NO)$ values of 2.0 (upper line) and 1.5 Å^3 (lower line). Use of the lower NO polarizability again yields a better fit to the experimental data, although the differences between the two calculated curves are not marked. (Inclusion of mild nonrandom CO/NO intermixing to the extent suggested from the above analysis alters the shape of these calculated $A_{NO}-X_{NO}$ curves only slightly.) Significantly, the experimental $A_{NO}-X_{NO}$ behavior is very different than the linear dependence observed for NO coadsorbed with water (open circles). This point is illustrated directly by the increases in the ν_{NO} band intensities observed upon removing the CO component, as clearly evident in Figure 9. Moreover, if the NO adsorption in the latter (water coadsorption) environment had been random (i.e., NO aggregation did not occur), one would expect to obtain nonlinear $A_{NO}-X_{NO}$ plots that are curved in the *opposite* direction, i.e., toward higher A_{NO} values, as observed (and predicted) for CO adsorption (Figure 7). [Such $A_{NO}-X_{NO}$ curvature is indeed obtained for NO coadsorption with water on Ir(110).[27,28]]

This $A_{NO}-X_{NO}$ dependence observed for the CO/NO mixtures, and its approximate consistency with the theoretical

predictions for either molecularly random or mildly nonrandom mixed adlayers, provides persuasive evidence of the occurrence of substantial "intensity transfer" (also termed "intensity-borrowing" or "intensity-stealing")[15a] from the lower to higher frequency band partners.[7a] We have observed roughly similar behavior also for mixed CO/NO adlayers on Ir(110)[7a] and Pt(100),[5] although interpretation of these systems is complicated somewhat by probable surface reconstruction and multiple adsorbate binding sites, respectively. The well-defined nature of the present Ir(111)/NO,CO system provides an unusual opportunity to examine the nature of such band intensity transfer in a more quantitative manner.

Briefly, the effect is a manifestation of dynamic dipole−dipole coupling between spatially juxtaposed adsorbate oscillators having significantly different singleton frequencies.[15,22,24] Physically, the observed shift of band intensity from the lower to higher frequency oscillators can be thought of as arising from the ability of the latter to screen the electric field in the vicinity of the former but not vice versa.[15] The effect is most familiar within mixed isotopic adlayers, such as $^{13}CO/^{12}CO$, which are commonly utilized to decouple the like-oscillator vibrations to yield "singleton" band frequencies in the absence of the wavenumber blueshifts caused by dipole coupling. While the latter effect on the observed adlayer band *wavenumbers* only occurs for oscillators having small (or zero) differences in singleton frequencies, $\Delta\nu_s$, the "dipole coupling-screening" effect on band *intensities*, i.e., band intensity transfer, can be substantial even for oscillator partners having moderate (several hundred cm^{-1}) $\Delta\nu_s$ values.[22,25] For example, this effect can account for the markedly (2−3-fold) larger intensity of the atop relative to the 3-fold hollow ν_{CO} bands in the compressed (2×2)−3CO adlayer on Pt(111) electrodes, even though the site occupancy of the latter (lower-frequency) oscillator is 2-fold *larger* than for the former (higher-frequency) component, and the singleton frequency difference is about 300 cm^{-1}.[25,26] While most attention has been devoted to band intensity transfer within pure chemisorbate (especially CO) layers having multiple oscillator frequencies associated with distinct binding sites, the effect is equally applicable to coadsorbed adlayers, as here, where the dissimilar oscillator frequencies are associated with different chemical species.

As noted in ref 7a, a virtue of simple coadsorbate systems, such as the present CO/NO adlayers, is the opportunity to examine the degree of intensity transfer as the density ratio of higher to lower frequency oscillators in the adlayer mixture is altered. One would expect the degree of intensity suppression, as evaluated by the "intensity-transfer factor" ITF $(= A_{NO}/A_{NO}^{\circ}$, vide supra), to be progressively enhanced as the lower-frequency (NO) oscillator is surrounded increasingly by the higher-frequency (CO) coadsorbate. Examination of the corresponding experimental data and dipole-coupling predictions (filled circles and solid traces, Figure 8) clearly shows that this is the case. Moreover, the reasonable agreement obtained between the shape of the experimental and calculated $A_{NO}-X_{NO}$ plots (Figure 8) provides additional evidence that the CO/NO adlayers are largely molecularly intermixed.

It is also interesting to examine the shape of the $A_{CO}-X_{CO}$ plots (Figure 7) in the context of band intensity transfer. The slightly enhanced A_{CO} values observed at intermediate and low X_{CO} values in the NO versus the water coadsorbate matrix (filled versus open circles, Figure 7) is consistent with the occurrence of NO band suppression due to intensity transfer. This is because the intensity "lost" from the lower-frequency feature should be transferred to the higher-frequency band. However, the intrinsically smaller absorbance of the former band should result in the effect upon the latter band intensity being disproportionately smaller. Differences between the A_{CO} values in the NO and water matrixes may also arise from variations in coadsorbate dielectric screening. Nevertheless, we emphasize that the markedly (even qualitatively) different effects on the $A_{NO}-X_{NO}$ and $A_{CO}-X_{CO}$ plots seen by switching from the single chemisorbate to the mixed CO/NO adlayers clearly indicate the presence of substantial band intensity-transfer effects in the latter environment.

It remains to consider the origins of the θ_{CO}−dependent ν_{CO} bandwidths in the water and NO matrixes. The dashed line in Figure 10 is the $\Delta\nu_{1/2}-\theta_{CO}$ plot obtained from the dipole-coupling simulations for CO adsorbed with water. These calculations assumed an "intrinsic" bandwidth of 10 cm^{-1} (chosen in part to match the limitingly high θ_{CO} values). The solid trace in Figure 10 is the corresponding simulated plot for the mixed CO/NO adlayers. Virtually the same calculated $\Delta\nu_{1/2}-\theta_{CO}$ plots were obtained when taking α_e(NO) to be either 2.0 or 1.5 $Å^3$ (vide supra). The progressive increases in the calculated $\Delta\nu_{1/2}$ values toward lower θ_{CO} reflect "stochastic broadening", arising physically from statistically random variations in the local CO coverage, and hence the degree of dipole−dipole coupling.[32] As a consequence, the calculated bands exhibit a "tail" toward lower wavenumbers and, thereby, yield larger $\Delta\nu_{1/2}$ values; such band shapes are also clearly evident in the experimental ν_{CO} spectra (Figure 1). This reflects a disproportionately larger contribution to the integrated band absorbance from the blueshifted ν_{CO} components arising from intensity stealing. The bandwidth *narrowing* seen toward higher θ_{CO} (open circles, Figure 10) arises on this basis from the progressively greater "intensity bias" toward the most blue-shifted oscillator components expected as the extent of dipole coupling increases, i.e., so-called coupling-induced "band narrowing" occurs.[34] The latter effect predicts that a narrow, approximately Lorentzian, band will occur for compressed adlayers, as observed experimentally for the Ir(111)/CO system in aqueous electrochemical[6] as well as UHV[14] environments.

One also might expect the occurrence of inhomogeneous band broadening, especially toward lower θ_{CO}, associated from increased solvation of the CO chemisorbate. However, such line broadening should also yield largely Gaussian-shaped bands, which are not observed (Figure 1). Moreover, even though such increasing "inhomogeneous solvation" of the CO adsorbate anticipated in the presence of coadsorbed water should not occur in the mixed CO/NO adlayers, these two environments yield similarly shaped $\Delta\nu_{1/2}-\theta_{CO}$ plots (Figure 10). Interestingly, the experimental $\Delta\nu_{1/2}-\theta_{CO}$ dependence within the coadsorbed NO matrix (filled circles, Figure 10) is also in very good agreement with dipole-coupling predictions (solid trace). Furthermore, the 3−4 cm^{-1} broader ν_{CO} bandwidths observed at intermediate CO coverages are nicely accounted for on this basis (Figure 10).

The larger $\Delta\nu_{1/2}$ values observed in the CO/NO adlayers can again be readily understood in terms of CO−NO dynamic dipole coupling and band intensity transfer. As noted above, the broadened ν_{CO} bands arise on this basis from statistical variations in the local CO population density, the lower-wavenumber tail being associated with more "isolated" CO molecules. These oscillators tend to lose intensity to nearby CO's having locally higher population densities (and hence blueshifted ν_{CO} frequencies), accounting for the "asymmetric tailed" band shape. In the coadsorbed NO matrix, however, these lower-frequency ν_{CO} band components also *gain* intensity by dynamic coupling with

surrounding NO oscillators. This intensity stealing will be more prevalent for the redshifted ν_{CO} components since they will be surrounded to a greater extent by NO molecules. Consequently, the intensity of low-wavenumber ν_{CO} components will be enhanced in the presence of coadsorbed NO relative to water since such coadsorbate−CO band intensity stealing will only occur in the former case. This band shape modification yields larger effective ν_{CO} bandwidths at intermediate θ_{CO} values, in harmony with experiment. This interpretation was supported further by model calculations where a single CO oscillator was surrounded by variable numbers (6−100) of either coadsorbed water or NO molecules. While the calculated ν_{CO} frequency remained within 1 cm^{-1} of the singleton value (vide supra), the ν_{CO} band intensity was determined to be about 20% higher in the presence of coadsorbed NO, reflecting the influence of band intensity transfer.

The NO bandwidths were not subjected to a detailed analysis in the CO/NO mixtures, in part because the observed $\Delta\nu_{1/2}$ values are relatively broad (ca. 30 cm^{-1}), even at high X_{NO} values. With coadsorbed water, the NO $\Delta\nu_{1/2}$ values increase to about 40 cm^{-1} toward low θ_{NO}. The low-wavenumber tail clearly evident at low NO coverages (Figure 2) likely arises from factors similar to those discussed above for CO, even though the near-θ_{NO} invariant peak ν_{NO} frequency implies the presence of chemisorbate clustering with coadsorbed water (vide supra). Interestingly, however, the observed NO bandwidths in the CO/NO mixtures *decrease* toward lower X_{NO} values (<0.5), so that $\Delta\nu_{1/2} \approx 15$ cm^{-1} at $X_{NO} \approx 0.2$. (Examination of lower NO coverages is thwarted by the intensity-transfer effect, yielding extremely small NO band absorbances, Figure 8). This $\Delta\nu_{1/2}-X_{NO}$ dependence, opposite to the CO oscillator case, is semiquantitatively mimicked by the spectra simulated from dipole-coupling calculations.

Concluding Remarks: Structural Implications

The present system provides an unusual opportunity to explore some facets of coadsorbate vibrational interactions and, hence, mixed adlayer structure at an ordered metal surface. In particular, the apparent presence of preferred atop (or near-atop) binding for CO and NO, both separately and together, on Ir(111) throughout the accessible range of coverages, as deduced from the simple infrared spectral fingerprints, enables insightful comparisons to be undertaken with the predictions of vibrational dipole-coupling calculations since only a pair of singleton oscillators (CO and NO) needs to be considered. This straightforward situation enables us to deduce, on the basis of composition-dependent vibrational band frequency and intensity data in comparison with the dipole-coupling predictions, the essentially *molecularly intermixed* nature of the CO/NO adlayers. Admittedly, a degree of nonrandom mixing may well occur, as indeed suggested by the improved fits to the experimental $\nu_{CO}-X_{CO}$ dependence obtained when some statistically preferred formation of locally CO-rich regions is included in the dipole-coupling simulations. However, it is important to recognize that the occurrence of truly segregated CO and/or NO domains, featuring locally *pure saturated* CO/NO islands, can essentially be eliminated on the basis of the present analysis. The presence of such islands, at least those having nanoscale (or larger) dimensions (say $>10-20$ molecules), would yield ν_{CO} and ν_{NO} bands within the coadsorbate mixtures that are insensitive to dilution by the other component, since the local dipole coupling will instead reflect chiefly CO−CO and NO−NO interactions (cf., ref 18). This is clearly not observed.

The simplest manifestation of the importance of CO−NO interactions is to be found in the marked ν_{CO}^{p} and ν_{NO}^{p} redshifts induced by dilution with NO and CO, respectively (Figures 4−6). However, important corroborating information is provided by both the composition-dependent band absorbance and bandwidth behavior (Figures 7, 8, 10). In particular, the observed marked degree of intensity transfer from the lower (NO) to higher (CO) band components, the extent increasing toward small X_{NO} values (Figures 8 and 9), constitutes persuasive evidence of the importance of CO−NO vibrational interactions within the mixed adlayers. The presence of largely intermixed CO/water adlayers, i.e., the occurrence of near-random θ_{CO}-dependent CO adsorption in the presence of coadsorbed water as well as NO, can also be diagnosed from the $\nu_{CO}^{p}-$, $A_{CO}-$, and $\Delta\nu_{1/2}-\theta_{CO}$ behavior in comparison with the dipole-coupling predictions, although the analysis is now determined only by CO−CO dynamic coupling and CO−CO and CO−water dielectric screening effects. In contrast to both the mixed CO/water and CO/NO adlayers, however, the NO/water system clearly involves considerable NO clustering. The equilibrium formation of intermixed, rather than segregated, binary (X−Y) adlayers simply requires that the X−Y interaction should be more favorable (or less unfavorable) than the average of the X−X and Y−Y interaction energies.[1a] Unfortunately, there is little information available regarding such interaction terms, especially for mixed coadsorbates. Nevertheless, interestingly marked differences in the CO−CO and NO−NO interactions on Pt(100) in UHV have been determined from calorimetry,[16] and the presence of weakly attractive CO/NO interactions on Pt(111) has been implied from desorption kinetic data.[35]

The occurrence of molecularly intermixed CO/NO adlayers has also been deduced, primarily from vibrational spectroscopy, on several low-index Pt-group surfaces in UHV,[1a] such as Pt(100),[36] even though the analyses are less quantitative than for the present system. We have recently made a similar structural deduction for CO/NO coadsorption on Pt(100) in aqueous solution,[5] as well as on Pt(111), Rh(100), and Pd(111).[7b] The phenomenon, therefore, appears to be quite widespread, at least for this coadsorbate pair. More generally, the present findings suggest the potentially broad-based value of dipole-coupling analyses in conjunction with vibrational spectroscopy as a useful means of exploring molecular coadsorbate structure. Given the general importance of coadsorption phenomena, especially in electrochemical systems, one can anticipate a more common use of this strategy in the future.

Acknowledgment. C.T. is grateful to the National Science Council of Taiwan for financial aid. This work was also supported by the U.S. National Science Foundation (to M.J.W.).

References and Notes

(1) For overviews, see: (a) White, J. M.; Akhter, S. *CRC Crit. Rev. Solid State Mater. Sci.* **1988**, *14*, 131. (b) Nørskov, J. K. In *The Chemical Physics of Solid Surfaces*; King, D. A., Woodruff, D. P., Eds.; Elsevier: Amsterdam, 1993; Vol. 6, Chapter 1.

(2) For reviews, see: (a) Nichols, R. J. In *Adsorption of Molecules at Electrodes*; Lipkowski, J., Ross, P. N., Eds.; VCH Publishers: Weinheim, 1992; Chapter 7. (b) Korzeniewski, C.; Severson, M. W. *Spectrochim. Acta* **1995**, *51A*, 499. (c) Iwasita, T.; Nart, F. C. *Prog. Surf. Sci.* **1997**, *55*, 271. (d) Weaver, M. J.; Zou, S. In Spectroscopy for Surface Science. *Advances in Spectroscopy*; Clark, R. J. H., Hester, R. E., Eds.; Wiley: Chichester, 1998; Vol. 26, Chapter 5.

(3) (a) Chang, S.-C.; Weaver, M. J. *J. Phys. Chem.* **1991**, *95*, 5391. (b) Villegas, I.; Weaver, M. J. *J. Phys. Chem. B* **1997**, *101*, 10166.

(4) Rodes, A.; Gómez, R.; Perez, J. M.; Feliu, J. M.; Aldaz, A. *Electrochim. Acta* **1996**, *41*, 729.

(5) Tang, C.; Zou, S.; Weaver, M. J. *Surf. Sci.* **1998**, *412/413*, 344.

(6) Tang, C.; Zou, S.; Severson, M. W.; Weaver, M. J. *J. Phys. Chem. B*, in press.

(7) (a) Weaver, M. J.; Tang, C.; Zou, S.; Severson, M. W. *J. Chem. Phys.* **1998**, *109*, 4135. (b) Zou, S.; Tang, C.; Chang, S.-C.; Weaver, M. J. *J. Electroanal. Chem.*, submitted for publication.

(8) Gómez, R.; Weaver, M. J. *J. Electroanal. Chem.* **1997**, *435*, 205.

(9) Gómez, R.; Feliu, J.; Aldaz, A.; Weaver, M. J. *Surf. Sci.* **1998**, *410*, 48.

(10) Chang, S.-C.; Weaver, M. J. *J. Chem. Phys.* **1990**, *92*, 4582.

(11) Corrigan, D. S.; Weaver, M. J. *J. Electroanal. Chem.* **1988**, *241*, 143.

(12) (a) Motoo, S.; Furuya, N. *J. Electroanal. Chem.* **1984**, *181*, 301. (b) Hoshi, N.; Uchida, T.; Miziuwa, T. *J. Electroanal. Chem.* **1995**, *381*, 261.

(13) Jiang, X.; Chang, S.-C.; Weaver, M. J. *J. Phys. Chem.* **1991**, *95*, 6453.

(14) Lauterbach, J.; Boyle, R. W.; Schick, M.; Mitchell, W. J.; Meng, B.; Weinberg, W. H. *Surf. Sci.* **1996**, *350*, 32; also see erratum in *Surf. Sci.* **1996**, *366*, 228.

(15) For reviews, see: (a) Hollins, P.; Pritchard, J. *Prog. Surf. Sci.* **1985**, *19*, 275. (b) Ueba, H. *Prog. Surf. Sci.* **1986**, *22*, 181. (c) Ryberg, R. *Adv. Chem. Phys.* **1989**, *76*, 1.

(16) Yeo, Y. Y.; Vattuone, L.; King, D. A. *J. Chem. Phys.* **1996**, *104*, 3810.

(17) Chang, S.-C.; Roth, J. D.; Weaver, M. J. *Surf. Sci.* **1991**, *244*, 113.

(18) Severson, M. W.; Weaver, M. J. *Langmuir* **1998**, *14*, 5603.

(19) Love, B.; Lipkowski, J. *ACS Symp. Ser.* **1988**, *378*, 484.

(20) (a) Chang, S.-C.; Weaver, M. J. *J. Phys. Chem.* **1990**, *94*, 5094. (b) Chang, S.-C.; Weaver, M. J. *Surf. Sci.* **1990**, *230*, 222. (c) Chang, S.-C.; Weaver, M. J. *J. Electroanal. Chem.* **1990**, *285*, 263.

(21) Tang, C.; Zou, S.; Severson, M. W.; Weaver, M. J. Manuscript in preparation.

(22) Persson, B. N. J.; Ryberg, R. *Phys. Rev. B* **1981**, *24*, 6954.

(23) Luo, J. S.; Tobin, R. G.; Lambert, D. K. *Chem. Phys. Lett.* **1993**, *204*, 445.

(24) Severson, M. W.; Stuhlmann, C.; Villegas, I.; Weaver, M. J. *J. Chem. Phys.* **1995**, *103*, 9832.

(25) (a) Leibsle, F. M.; Sorbello, R. S.; Greenler, R. G. *Surf. Sci.* **1987**, *179*, 101. (b) Brandt, R. K.; Sorbello, R. S.; Greenler, R. G. *Surf. Sci.* **1992**, *271*, 605.

(26) Moskovits, M.; Hulse, J. E. *Surf. Sci.* **1978**, *78*, 397.

(27) Unlike the present Ir(111)/NO system, NO adsorption on Ir(110) in 0.1 *M* $HClO_4$ yields sizable $\nu_{NO}{}^{p}$ blueshifts (40−50 cm^{-1}) with increasing θ_{NO}, consistent with near-random NO adsorption.[28] The present $\nu_{NO}{}^{s}$ estimate on Ir(111), 1800 cm^{-1}, was therefore obtained by combining the high θ_{NO} $\nu_{NO}{}^{p}$ value with this θ_{NO}-dependent frequency shift.

(28) (a) Gómez, R.; Weaver, M. J. *Langmuir* **1998**, *14*, 2525. (b) Tang, C.; Zou, S.; Weaver, M. J. Manuscript in preparation.

(29) Persson, B. N. J.; Liebsch, A. *Surf. Sci.* **1981**, *110*, 356.

(30) Hasted, J. B. In "*Water—A Comprehensive Treatise*; Franks, F., Ed.; Plenum: New York, 1972; Vol. 1, Chapter 7.

(31) Villegas, I.; Weaver, M. J. *J. Chem. Phys.* **1994**, *101*, 1648.

(32) It should be noted, however, that additional stochastic band-broadening effects arising from a statistical distribution of adsorbate binding sites, and therefore varying singleton frequencies $\nu_{CO}{}^{s}$, are not included in these calculations; only a *single* $\nu_{CO}{}^{s}$ value (2000 cm^{-1}) was employed. [While the latter stochastic broadening contribution was found to exert a significance influence on the bandwidths for multifold-coordinated CO,[24] it should be markedly less important for atop (or near atop) CO geometries,[33] as encountered here.]

(33) Schweizer, E.; Persson, B. N. J.; Tüshaus, M.; Hoge, D.; Bradshaw, A. M. *Surf. Sci.* **1989**, *213*, 49.

(34) (a) Persson, B. N. J. *J. Electron Spectrosc. Related Phenom.* **1990**, *54/55*, 81. (b) Persson, B. N. J.; Hoffman, F. M. *J. Electron Spectrosc. Related Phenom.* **1987**, *45*, 215.

(35) Skelton, D. C.; Wei, D. H.; Kevan, S. D. *Surf. Sci.* **1996**, *355*, L319.

(36) Gardner, P.; Martin, R.; Tüshaus, M.; Bradshaw, A. M. *Surf. Sci.* **1992**, *269/270*, 405.